Proceedings of 2008 ASME Summer Heat Transfer Conference
HT2008
August 10-14, 2008, Jacksonville, Florida USA

HT2008-56077

CFD Approach Analysis of Chemical Reactions Coupled Convective Heat Transfer in Reformer Ducts

Jinliang Yuan
Dept. of Energy Sciences, Faculty of Engineering
Lund University, Box 118, 22100 Lund, Sweden

Guogang Yang
Marine Engineering College, Dalian
Maritime University, Dalian 116026, China

Bengt Sundén
Dept. of Energy Sciences, Faculty of Engineering
Lund University, Box 118, 22100 Lund, Sweden

ABSTRACT

Thermo-mechanical failure of components in a compact steam reformer is a major obstacle to bring this technology to real-life applications. The probability of material degradation and failure depends strongly on the convective heat transfer in the fuel gas flow duct and local temperature distribution in multi-functional materials. It is of significant importance to accurately predict the convective heat transfer coupled with catalytic reactions within the reformer components.

In this paper, the simulation and analysis of combined chemical reactions and transport processes are conducted for a duct relevant for compact design steam reformer, which consists of a porous layer for the catalytic reforming reactions of methane, the fuel gas flow duct and solid plates. A fully three-dimensional computational fluid dynamics (CFD) approach is applied to calculate transport processes and effects of thermal conductivities of the involved multi-functional materials on convective heat transfer/temperature distributions, in terms of interface temperature gradients/heat fluxes and Nusselt numbers. The steam reformer conditions such as mass balances associated with the reactions and gas permeation to/from the porous anode are implemented in the calculation. The results show that the classic thermal boundary conditions (either constant heat flux or temperature, or combined one) may not be applicable for the interfaces between the fuel flow duct and solid plate/porous layer.

INTRODUCTION

Methane is usually converted into H_2, CO and CO_2 by employing Ni as a catalyst supported by alumina in the reformers. Such reformers have been extensively developed in the last decays. In general, technologies to produce hydrogen from methane are based on one of the following processes: steam methane reforming (SMR), partial oxidation (POX) and autothermal reforming (ATR). There is an increasing interest worldwide in the development of innovative fuel processing technologies for fuel cell systems, for instance, compact reformers (CR hereafter) for a variety of applications. The basic idea of the CR is to catalytically activate both sides of a compact heat exchanger – one side for combustion to provide heat for the other side to sustain steam reforming of methane and produce hydrogen. In this configuration, the thin coating results in small thermal conduction and species diffusion path lengths that largely eliminate heat and mass transfer restrictions associated with conventional reformers, and an improved utilization of the intrinsic reforming catalyst kinetics is possible to achieve an efficient heat transfer. The compact reformer concept could lead to major applications in fuel cell systems for stationary and transportation applications [1, 2]. For instance, coupling of steam reforming and catalytic combustion in adjacent ducts have received attention recently, and an excellent review can be found in [3] regarding the CR concept application and new design development. As revealed in [3, 4], a majority of reformer literature is devoted to its steam reforming reaction kinetics, materials for the components and catalyst forming/distribution. Literature review shows that research on convective heat transfer involving catalytic chemical reactions is very limited.

Thermal management of typical reactors can be supplemented via the forced convective behavior of excessive gas flows in the ducts. In most cases, the characteristics of convective flow and heat transfer has been modeled after he classical duct flow problem with either uniform wall flux or wall temperature conditions. This is a rather gross assumption because the catalytic reforming reaction rates are closely coupled with fuel gas flows and heat transfer through and over the porous layers. As a consequence, the interface boundary conditions and convective heat transfer coefficients are significantly altered. As expected, the thermal properties of multi-functional materials may have certain effects on the catalytic reactions and the convective heat transfer.

The objective of this study is to investigate the complex and conjugated fuel gas convective heat transfer behavior in the flow duct and in the catalytic porous layer, along with the

reforming reactions and attendant species transport in a reformer duct. A three-dimensional computational procedure has been developed to simulate and analyse steam reforming of methane in a composite domain consisting of a porous active layer, a gas flow duct and solid plates. Momentum and heat transport together with fuel gas species equations have been solved with coupled source terms and variable thermo-physical properties (such as local density, viscosity, specific heat, etc.) of the fuel gas mixture. The results from this study provide insights into the convective heat transfer behavior of fuel gas flows and lead to the possible optimization of the thermal management design of compact fuel reformer.

PROBLEM STATEMENT AND MATHEMATICAL MODELING

There are several transport processes (such as mass, heat and momentum transport) together with chemical reactions appearing in multifunctional reactors. It is often found that the endothermic and exothermic reactions, such as hydrocarbon cracking, steam reforming and dehydrogenation, are strongly coupled by heat transfer in the reactors.

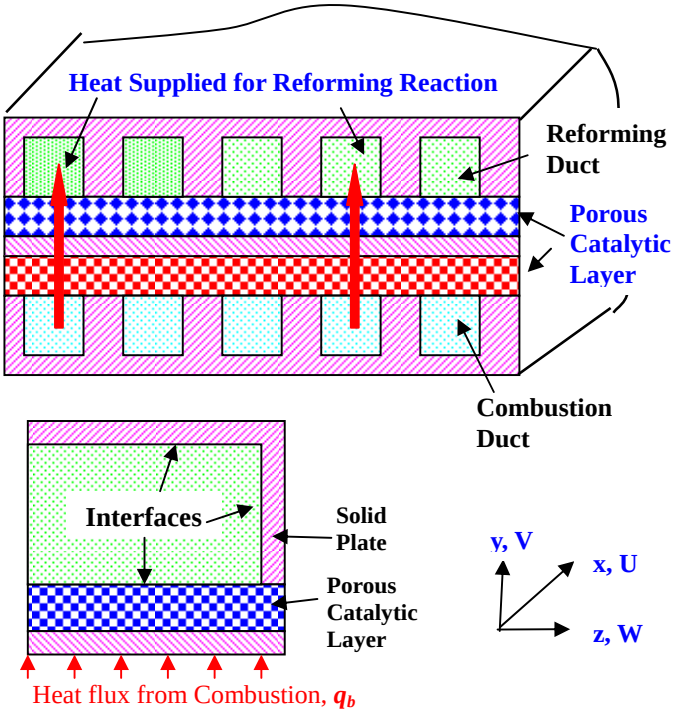

Figure 1. Scheme of unit reactors (up); and an investigated duct of steam reforming reactors.

A three-dimensional computational fluid dynamics (CFD) code was used to simulate a methane reforming duct from a typical compact reformer, as shown in Fig. 1. As revealed in [3, 4], the steam reforming, water gas-shift, and reverse methanation reactions of methane are the major ones with significant reaction rates. Consequently, only the following major chemical reactions are included in this study:

Methane steam reforming:

$$CH_4 + H_2O \rightarrow CO + 3H_2, \quad \Delta h_{(298K)} = 226000 \text{ kJ/kmol} \qquad (1)$$

Water gas-shift:

$$CO + H_2O \rightarrow CO_2 + H_2, \quad \Delta h_{(298K)} = -41000 \text{ kJ/kmol} \qquad (2)$$

Reverse methanation:

$$CH_4 + 2H_2O \rightarrow CO_2 + 4H_2, \quad \Delta h_{(298K)} = 165000 \text{ kJ/kmol} \qquad (3)$$

It should be mentioned that the above processes in Eqs. (1) and (3) are endothermic and the overall balance of the reactions requires net heat input. In general, this heat supply depends on the thermal integration methods employed and the associated combustion processes.

In a catalytic reformer, the governing equations to be solved are the mass, momentum, energy and species conservation equations. The mass continuity equation is written as

$$\nabla \bullet (\rho_{eff} \mathbf{V}) = 0 \qquad (4)$$

The momentum equation reads

$$\nabla \bullet (\rho_{eff} \mathbf{V}\mathbf{V}) = -\nabla P + \nabla \bullet (\mu_{eff} \nabla \mathbf{V}) + S_{di} \qquad (5)$$

The inclusion of the source term S_{di} allows Eq. (5) to be valid for both the porous catalytic layer and the fuel gas flow duct:

$$S_{di} = -(\mu_{eff} \mathbf{V} / \beta) \qquad (6)$$

This accounts for the linear relationship between the pressure gradient and flow rate according to Darcy's law. β is the porous layer permeability, and $\mathbf{V}$ represents the volume-averaged velocity vector of the species mixture. For example, the volume-averaged velocity component U in the x direction is equal to εU_p, where ε is the porosity and U_p the average pore velocity (or interstitial velocity).

In the fuel flow duct, the source term S_{di} becomes zero because the permeability β is infinite. Equation (5) then reduces to the regular Navier-Stokes equation. For the porous layer, the source term is not zero. Based on the thermal equilibrium assumption for the porous catalyst layer, only one energy equation is solved for the fuel gas species and the solid matrix:

$$\rho_{eff} c_{p,eff} \nabla \bullet (\mathbf{V}T) = \nabla \bullet (k_{eff} \nabla T - \sum_{i=1}^{n} \dot{\mathbf{m}}_i h_i) + S_T \qquad (7)$$

Equation (7) balances the convected energy, the heat conduction through the solid and the fuel gas mixture, the energy due to fuel gas species diffusion, and a source term S_T. In Eq. (7) h_i is the partial enthalpy of the ith species and reads:

$$h_i = h_{form,i} + \int_{T_0}^{T} c_{pi}(T)dT \quad (8)$$

where $h_{form,i}$ is the specific enthalpy of formation of the ith gas species at $T = T_0 = 298.15$ K. The heat source term S_T in Eq. (7) is associated with the steam reforming, water gas-shift and reverse methanation reactions,

$$S_T = \sum_i R_i \Delta h_{reaction,i} \quad (9)$$

where R_i is the reaction rate, and $\Delta h_{reaction,i}$ is the reaction enthalpy. The species mass conservation equations are written in the general form,

$$\nabla \bullet (\rho_{eff} \mathbf{V} Y_i) = \nabla \dot{m}_i + S_{s,i} \quad (10)$$

where Y_i is the mass fraction of the ith fuel gas species, $\dot{m}_i$ represents the mass diffusive flux of species, and $S_{s,i}$ the production/consumption rate of the ith fuel species. The above equation is solved for H_2, CH_4, CO and H_2O, respectively, i.e., for n-1 species where n is the total number of species involved in the fuel gas mixture. The mass fraction of the n^{th} species (CO_2) can be obtained from the requirement that the sum of the mass fractions equals one.

Mass diffusion is a process leading to equalization of substance fraction or establishing an equilibrium gas distribution that results from random migration of the species. The diffusion coefficients of species i in the gas mixture for the fuel gas flow duct are calculated by the expression based on the binary coefficients

$$D_{A,gm} = \frac{1 - X_A}{X_B / D_{AB} + X_C / D_{AC} + \ldots} \quad (11)$$

where $D_{A,gm}$ is the diffusion coefficient of the component A in the mixture with B, C, …, while X_A, X_B, X_C are the molar fraction of the appropriate species, and D_{AB} and D_{AC} the diffusion coefficients in the AB and AC binary system, respectively. It is clear that for an n component system, $n(n-1)/2$ binary diffusivities are required.

For the porous catalytic reaction layer, Knudsen diffusion occurs in porous layer with small pores or under low pressure when the mean free-path of molecules is larger than the pore size, and the molecules collide with the walls more often than between themselves. In order to calculate the Knudsen diffusion flux, the coefficient $D_{i,k}$ is calculated based on the free molecule flow theory

$$D_{i,k} = \frac{2}{3} r_e v_i = \frac{2}{3} r_e \sqrt{\frac{8\Re T}{\pi M_i}} \quad (12)$$

in which r_e is the effective radius and v_i the average molecular speed of the ith gas species. To account for the reduction in the cross-sectional area and the increased diffusion length due to the tortuous paths of real pores in the porous catalytic layer, the effective diffusion coefficient can be evaluated:

$$D_{i,eff} = \frac{\varepsilon}{\tau}\left(\frac{D_{i,gm} \times D_{i,k}}{D_{i,gm} + D_{i,k}}\right) \quad (13)$$

where ε is the porous porosity, and τ the tortuosity. In Eq. (10), the source terms $S_{s,i}$ read:

$$\begin{aligned} S_{s,H_2} &= (3R_1 + R_2 + 4R_3)M_{H_2}; S_{s,CH_4} = (-R_1 - R_3)M_{CH_4}; \\ S_{s,H_2O} &= (-R_1 - R_2 - 2R_3)M_{H_2O}; S_{s,CO} = (R_r - R_s)M_{CO} \end{aligned} \quad (14)$$

where R_i is the chemical reaction rate expressed by following Eqs. (15-17).

The catalytic reforming reactions are coupled with the mass, momentum, heat and species transport in the model. There exist various reaction kinetics and rate/equilibrium constants reported in the literature for the reactions. A general rate equation based on Langmuir-Hinselwood-Hougen-Watson (LHHW) approach [3-7] describes most accurately the process for a wide range of parameters, and is applied in this study to express the kinetic rates of absorption or production of the gas species, based on partial pressure, temperature and species compositions for the chemical reactions (15)-(17):

$$R_1 = \frac{\frac{k_1}{p_{H_2}^{2.5}}\left(p_{CH_4} p_{H_2O} - \frac{p_{H_2}^3 p_{CO}}{K_{e,1}}\right)}{(\mathrm{Den})^2} m_{cl}, \ \mathrm{kmol/(m^3 s)} \quad (15)$$

$$R_2 = \frac{\frac{k_2}{p_{H_2}}\left(p_{CO} p_{H_2O} - \frac{p_{H_2} p_{CO_2}}{K_{e,2}}\right)}{(\mathrm{Den})^2} m_{cl}, \ \mathrm{kmol/(\ m^3 s)} \quad (16)$$

$$R_3 = \frac{\frac{k_3}{p_{H_2}^{3.5}}\left(p_{CH_4} p_{H_2O}^2 - \frac{p_{H_2}^4 p_{CO_2}}{K_{e,3}}\right)}{(\mathrm{Den})^2} m_{cl}, \ \mathrm{kmol/(\ m^3 s)} \quad (17)$$

in which, m_{cl} is the catalyst loading (kg_{cat}/m^3), and $\mathrm{Den} = 1 + K_{CO}p_{CO} + K_{H2}p_{H2} + K_{CH4}p_{CH4} + K_{H2O}p_{H2O}/p_{H2}$. The values of the pre-exponential factors, activation energies, equilibrium constants, and heat of adsorption are given in Table 1 and Table 2, respectively.

Table 1. Kinetic parameters and equilibrium constants [3].

Reactions	Kinetic rate constant k_i (kmol/kg_{cat}h)	Equilibrium constant K_{ej}
Steam reforming	$4.225\times10^{15}\times e^{(-240100/RT)}$	$5.75\times10^{12}\times e^{(-11476/RT)}$, bar^2
Water gas-shift	$1.955\times10^{6}\times e^{(-67130/RT)}$	$1.26\times10^{-2}\times e^{(4639/RT)}$
Reverse methanation	$1.02\times10^{15}\times e^{(-243900/RT)}$	$7.24\times10^{10}\times e^{(-21646/RT)}$, bar^2

Table 2. Adsorption constants K_i [3].

Species	CH_4	CO	H_2	H_2O
K_i	$6.65\times10^{-4}\times e^{(-38280/RT)}$, bar^{-1}	$8.23\times10^{-5}\times e^{(-70650/RT)}$, bar^{-1}	$6.12\times10^{-9}\times e^{(-82900/RT)}$, bar^{-1}	$1.77\times10^{5}\times e^{(88680/RT)}$, -

The governing equations above are coupled by temperature, partial pressure/fraction of gas species via source terms and local thermal-physical properties. It is clear that no gas flow is present in the solid plates. Eqs. (4), (5) and (10) are then blocked out and only the heat conduction equation, derived from the energy Eq. (7), is solved for these domains. Based on the reforming reaction function, the typical velocities, fuel gas mass fraction/flux boundary conditions are specified at the external walls (not at the interfaces) in this study. While for the temperature boundary conditions, the thermal insulation are put on the three walls (the top wall and the two side ones), and a constant heat flux condition is specified at the bottom wall (see Fig. 1), i.e.,

at the bottom wall ($y = 0$):

$$U = V = W = 0;\ q_b = \text{c};\ J_i = 0 \quad (i = H_2, CO, H_2O \text{ and } CH_4) \tag{18}$$

at the top and side walls:

$$U = V = W = 0,\ q = 0,\ J_i = 0 \tag{19}$$

at the mid-plane (z=a/2):

$$\frac{\partial U}{\partial z} = \frac{\partial V}{\partial z} = W = \frac{\partial T}{\partial z} = \frac{\partial Y_i}{\partial z} = 0 \tag{20}$$

It is very interesting to point out that the thermal conditions at the top and side interfaces are implicitly obtained by thermal coupling through the top/side interfaces, while all the conditions at the bottom interface (between the flow duct and the porous layer in Fig. 1) by coupling the mass, heat and species transfer. As revealed in this study, the obtained thermal conditions at the interfaces are characterized by axially varying wall-heat-fluxes (or temperature gradients) and wall-temperatures. As expected, it is due to the complex hydrodynamic and thermal transport interactions between the catalytic reaction-rates, species flux through the porous reaction layer, and the convective flows in the fuel gas duct.

Given the convective mass, flow, and temperature distribution fields, described by the governing equations above, the thermal performance at the interfaces can be evaluated by the average interface temperature and its gradient, or by the dimensionless Nusselt number. The Nusselt number Nu_i at the interface is:

$$\overline{Nu}_i = \frac{\bar{h}_i D_h}{k_{eff}} = \frac{(dT/dx)_i D_h}{(\overline{T}_i - T_{bulk})} \tag{21}$$

$\overline{T_i}$ is the spanwise average temperature at the interface i, $(dT/dx)_i$ the interface temperature gradients, T_{bulk} the mean stream-wise gas flow temperature in the cross-section,

$$T_{bulk} = \frac{\int T|U|dA}{\int |U|dA} \tag{22}$$

As mentioned earlier, the local thermal-physical properties of the gas mixture are variable. These parameters depend on the position in the duct, and the species mass fraction and/or temperature as well. Fuel gas mixture density, viscosity, thermal conductivity and specific heat are then calculated and updated during the calculations. It is worth to note that the approach applied in this study is based on one set of governing equations with the extra source terms and the local transport properties' implementation, which enables the porous reaction and pure fluid flow regions to be treated as a single domain. This approach has been successfully used in the fuel cell and reformer modeling society, particularly for cases involving the composite domains as in this study.

NUMERICAL SOLUTION METHOD-CFD APPROACH

A three-dimensional CFD code is applied. It is a general purpose one and is based on the finite-volume technique with boundary fitted coordinates for solving the differential equations. The Cartesian coordinate system in the physical space is replaced by a general non-orthogonal coordinate system. The momentum equations are solved for the velocity components on a non-staggered grid arrangement. The Rhie-Chow [8] interpolation method is used to compute the velocity components at the control volume faces. Algorithms based on the TDMA (Tri-Diagonal Matrix Algorithm) and a modified SIP (Strongly Implicit Procedure) are employed for solving the algebraic equations. In this study, the convective terms are treated by the QUICK (Quadratic Upstream Interpolation Convective Kinematics) scheme, while the diffusive terms are treated by the central difference scheme. The SIMPLEC (Semi-Implicit Method for Pressure-Linked Equations-Consistent) algorithm handles the linkage between velocities and pressure.

A uniform grid point distribution over the cross section is used. To obtain finer meshes in the entrance region of the duct, a non-uniform distribution of grid points with an expansion factor is implemented for the main flow direction. Various values of the expansion factor have been checked and 1.01 (i.e., $\Delta x_{i+1}/\Delta x_i = 1.01$) was found to be sufficient to capture sharp parameter changes in the entrance region. During the iterative sequence, convergence is assessed at the end of each iteration on the basis of the residual sources criterion which compares the sum of the absolute residual source over all the control volumes in the computational domain, for each finite-

volume equation. The residual criterion is set to 10^{-5} in this study.

In order to evaluate the performance of the numerical method and code, test calculations considering grid sensitivity, code performance and validation were carried out. It has been found that the predictions do not change significantly in terms of fuel species distributions, when the number of grid points is increased beyond 70×70×50 (70×50 for the cross section, 70 for the main flow direction). Calculations have been carried out for fully developed conditions in a parallel plate duct for various thicknesses of the porous layer and the same boundary conditions of constant heat flux on the walls, see [6].

RESULTS AND DISCUSSION

Configuration and operating parameters of a typical reformer duct are applied as a base case in this study. Table 3 shows the duct geometries. For the porous layer, the parameters are chosen as: porosity ε = 0.5, permeability $\beta=2\times10^{-10}$ m^2, and catalyst loading mcl=1g$_{cat}$/cm^3. Fuel inlet temperature T_{in}=650^{o}C; inlet mole fraction H_2:CH_4:CO:H_2O:CO_2=0.026 :0.2470:0:0.7145:0.0125 with U_{in}=5m/s. The thermal conductivities are k_s=25.5 W/(mK) for the solid plates and k_p=3.0 W/(mK) for the catalyst and the supporting materials in the porous layer. It should be noted that all the results presented hereafter are for the base case condition unless otherwise stated.

Table 3. Geometries of the reforming reaction duct (cm).

	Length (x)	*Depth* (y)	*Width* (z)
Overall Duct	20	1	0.5
Fuel Flow Duct	20	0.4	0.4
Porous Layer	20	0.4	0.5

Figure 2*a* shows temperature distribution profiles along the main flow direction and for various cross-sections of the fuel reforming duct. It should be mentioned that the *x*-axis is plotted dimensionally, but *y*- and *z*-axes are plotted non-dimensionally with the duct height *h*. It is simply for the purpose to compare the predicted results from the parameter studies when the fuel duct and the porous layer cross-sectional geometries are varied (while *h* is kept constant). It is clear that the temperature increases steadily along the main flow direction in Fig. 2a. The variation in temperature distribution can also be observed in the vertical direction with a larger value at the bottom solid plate. These are created by the heat flux supplied by the catalytic combustion (modelled by a constant heat flux q_b=1000 J/(m^{2}s) in this study). It is also clear that the temperature change is more sharply distributed in the solid plates compared to the ones within the porous layer and gas flow duct. It is due to the fact that the solid plate thermal conductivity is bigger than the local values in other components. As expected the thermal resistances of the solid plates are smaller.

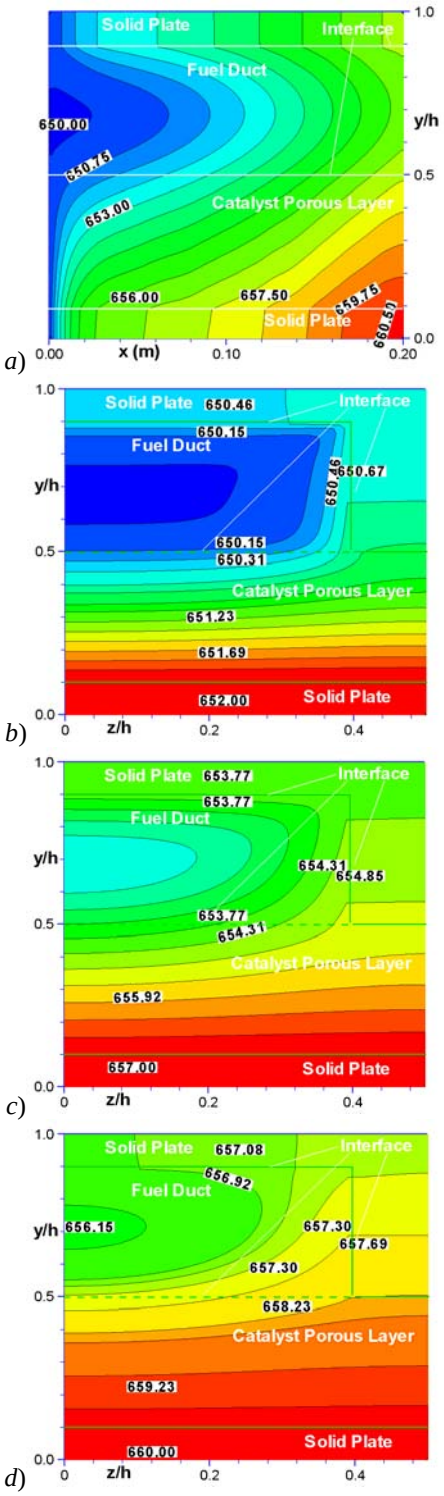

Figure 2. Temperature contours: a) along main flow direction; at the cross sections of: b) entrance; c) half length from the inlet; d) outlet of the fuel reforming duct.

The cross-sectional temperature distributions are plotted in Fig. 2b-d for various stations. It is found that, in a cross

section, the temperature profile has maximum values close to the bottom solid plate, which is caused by the supplied heat flux at the bottom wall (in Fig. 1). It is obvious that almost uniformly distributed temperatures can be found in the solid plates and the porous catalyst layer. However, a bigger value has been predicted in the porous layer close to the side wall. On the other side, the thermal boundary layer development can be found in the gas flow duct, in which a distortion is observed close to the bottom interfaces due to the gas permeation into/from the porous layer, and thermal interactions across the interfaces [6].

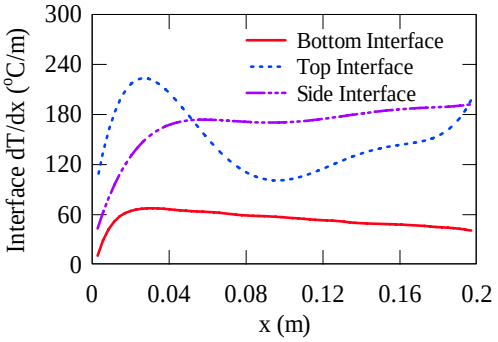

a)

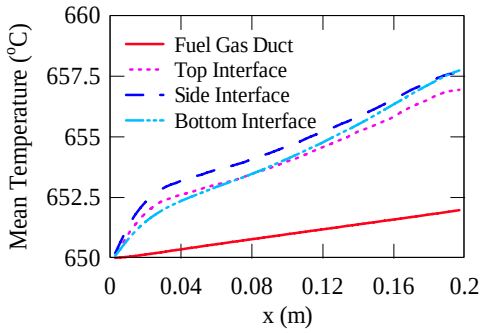

b)

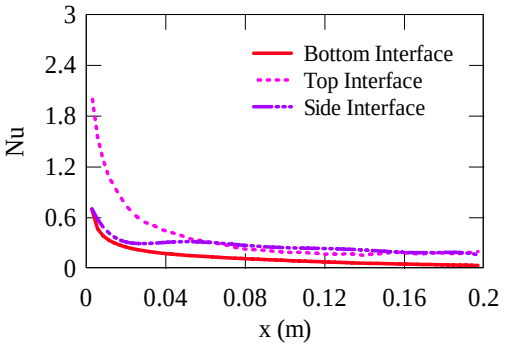

c)

Figure 3. a) Temperature gradient; b) temperature distribution, and c) Nu at the interfaces along the main flow reformer duct. Base case.

A noteworthy feature of the conjugate calculation and analysis in the current study is the characterization of the thermal boundary condition development close to the interfaces between the gas flow duct and the solid plates/the porous layer. It is achieved by the coupling of the mass, momentum, heat and fuel gas species with the catalytic chemical reactions. As shown in Figs. 3a and b, the averaged temperature gradient (or heat flux) and temperature distributions at the top, side and bottom interfaces (Fig. 1) are axially increased along the main flow direction, and they essentially describe the convective thermal boundary layer development in the fuel gas flow duct.

As shown in Fig. 3b, the interface and fuel gas bulk temperatures increase monotonically along the main flow direction. It is clearly evident that the interface temperatures are higher than that of the fuel gas, i.e., the fuel gas flowing in the duct is getting heated along the main stream. However the temperature gradients at the interfaces display different trends, as shown in Fig. 3a. The temperature difference across the top interface is getting bigger at the entrance, and decreases after a peak value until a low value reached at the middle of the duct length from the entrance. It displays monotonically an increase afterwards. However the temperature gradients at the side and bottom interfaces show more stable variations, i.e., increase sharply from the duct entrance, and maintain almost stable values until the duct outlet. The consequent impact of the altered temperatures and the interface temperature gradients on the convective heat transfer coefficient or Nu is plotted in Fig. 3c.

It is obvious that the classical duct thermal boundary conditions (constant heat flux or wall temperature or the combined ones on the walls) are not rigorously applicable in the chemical reaction coupled gas flow and heat transfer, such as in this study, in which the heat source/sink in the porous materials and the heat conduction in the solid plates are involved. It is revealed that the real thermal interface represents axial variations in both the wall heat flux (or the interface temperature gradient) and surface temperature due to the involved chemical reactions and heat supply, which requires a conjugate treatment of the mass transfer, gas flow, heat transport and chemical reactions in various functional components.

The thermal conductivities of the functional components are quite differently applied in the literature depending on different materials. In this study, simulation was conducted for the values of 3 and 25.5 W/(mK) for the porous layer solid matrix and the solid plate material, respectively. However, a parameter study is conducted to investigate the thermal conductivity effects on the temperature distribution and convective heat transfer.

Special attention is then paid to evaluate the influence of thermal conductivity on the convective heat transfer in the fuel gas flow duct and temperature distribution within the functional components in this study. The simulations are done under the same standard conditions except the thermal conductivities of the porous layer and the solid plates. For the case of low

thermal conductivities, k_p=0.6 and k_s=5 W/(mK) for the porous layer and the solid plates, respectively, the maximum temperature (691°C vs. 655°C reached in the bottom solid plate close to the exit) is bigger compared to that of high thermal conductivities, k_p=15 and k_s=125 W/(mK), as shown in Figs. 4a and b. Moreover, the porous layer and the bottom solid plate with higher temperatures can be observed in Fig. 4a with small thermal conductivities. This is mainly due to the fact that the heat supply to compensate the steam reforming reactions can not be effectively transported by thermal conduction in the bottom solid plate and further heat transfer in the porous layer due to small thermal conductivities. That implies a slow cooling process by the reaction related heat consumption in the porous layer. For the case of big thermal conductivities, the heat conduction becomes quick enough to balance the heat supply and the heat consumption, the maximum temperature then decreases, as shown in Figure 4b.

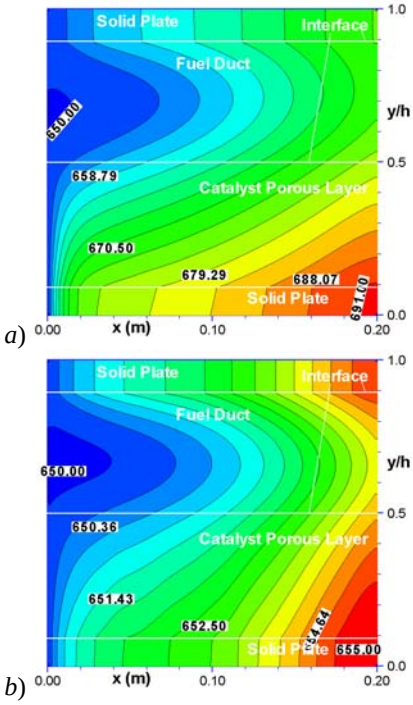

Figure 4. Temperature contours along the main flow direction by: a) small; and b) big thermal conductivities.

Table 3 Effects of thermal conductivity.

Thermal conductivity, W/(mK)	Methane Conversion Rate, %
k_p=0.6 and k_s=5	77.3
k_p=3 and k_s=25.5	69.5
k_p=15 and k_s=125	68.7

As a consequence, more significant impacts on the reforming reaction performance are expected for the case of the low thermal conductivities, k_p=0.1 and k_s=5 W/(mK). As revealed in the previous studies, the methane conversion rates are affected by various design and operating parameters, such as local temperature distribution in the porous layer, such as high temperature promotes big methane conversion rate. This trend is reflected in Table 3 as well.Figure 5 shows the effects of the thermal conductivities on the convective heat transfer close to the top interface (between the fuel gas flow duct and the top solid plate). As revealed in Fig. 3, the variation of the thermal boundary development at the top interface is prominent, in terms of variation of the interface temperature gradient and the cross-section averaged temperature distribution or the temperature difference between the top interface and bulk gas in the flow duct. This trend is enhanced if the small thermal conductivities (k_p=0.6 and k_s=5) are employed, as shown in Fig. 5a and b, respectively. Consequently, the convective heat transfer or Nu varies more significantly for the case of the small thermal conductivities, as shown in Fig. 5c.

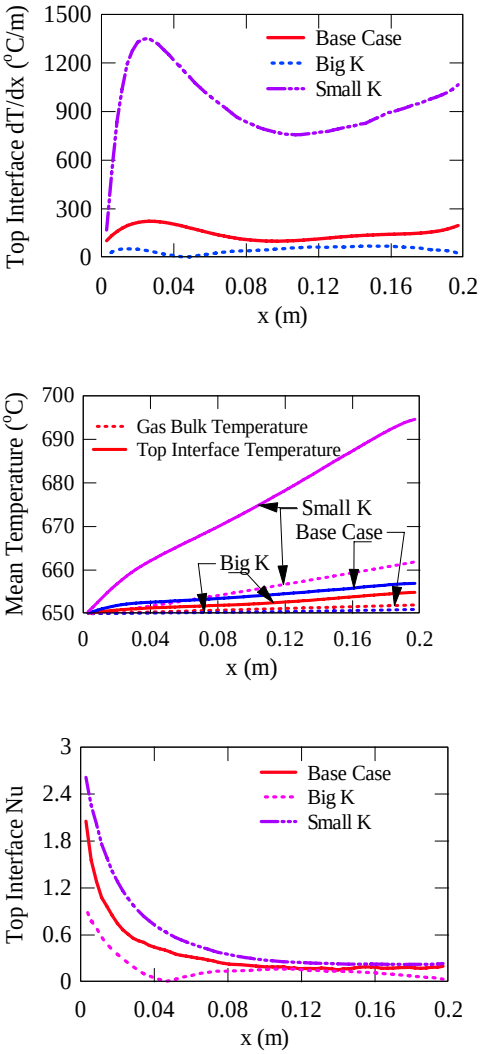

Figure 5. Thermal conductivity effects on: a) Temperature gradient; b) temperature profile; c) Nu at top interface along the main flow reformer duct.

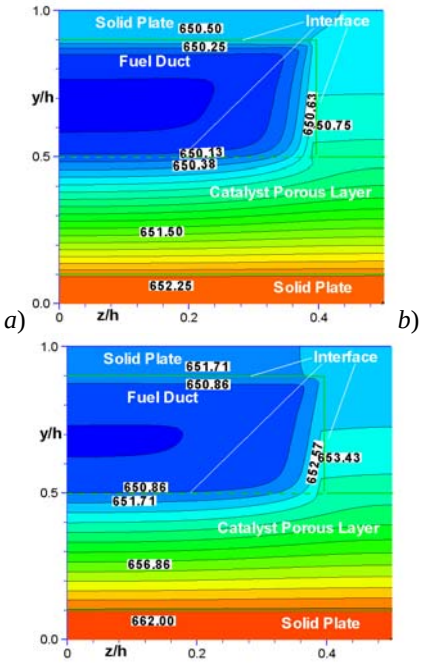

Figure 6. Temperature contours at the entrance cross-section by: a) big thermal conductivity; b) small thermal conductivity.

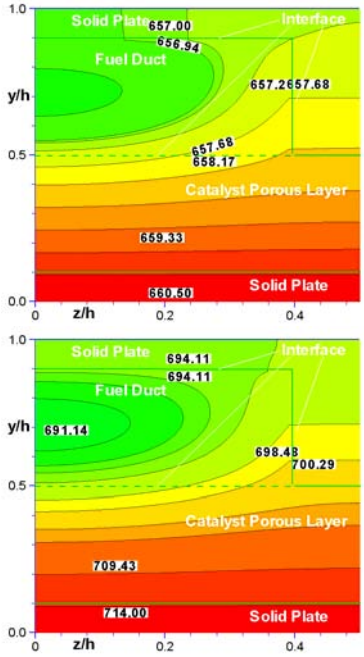

Figure 7. Temperature contour at outlet cross-sections by: a) big thermal conductivity; b) small thermal conductivity.

As shown in Figs. 6 and 7, the fuel gas temperature in the flow duct is heated by the surrounding interfaces for all thermal conductivities employed for the functional components. The temperature distribution at the cross-section close to the entrance is shown in Fig. 6, while Fig. 7 shows those of the outlet cross-sections. It is clear that the temperature differences between the solid plate/porous layer and the fuel gases cross the interfaces become more prominent for small thermal conductivities, as shown in Figs. 6a and b for the case of the entrance cross-sections. However, this characteristic is not significant for the cross-sections at the outlet, as shown in Fig. 7. A similar trend can be found for the case close to the side interface (not shown in this study).

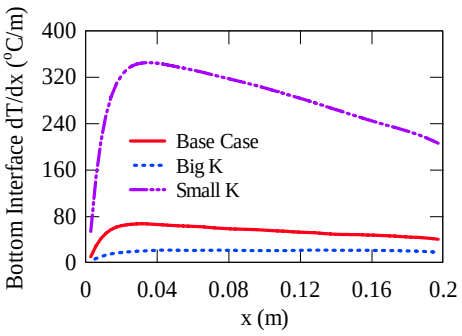

a)

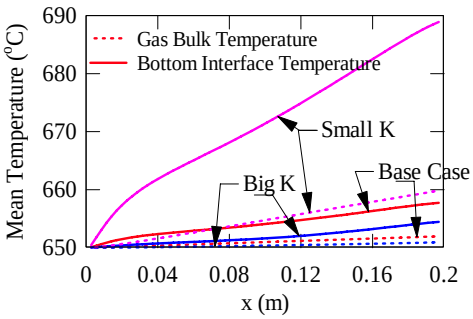

b)

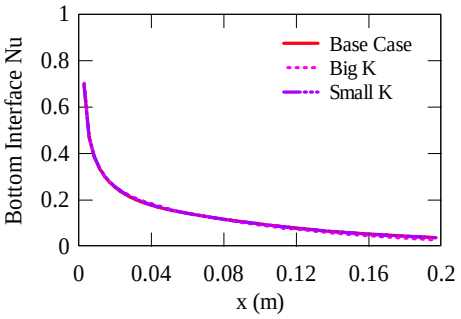

c)

Figure 8. Thermal conductivity effects on: a) temperature gradient; b) temperature profile; c) Nu at bottom interface along the main flow reformer duct.

It is interesting to point out that the averaged temperature gradient and temperature distributions at the bottom interface are axially varied in a similar way as for the top and side interfaces, i.e., small thermal conductivities hold prominent effects on the thermal condition development, as shown in Figs. 8a and b. However, the convective heat transfer coefficients are almost the same as plotted in Fig. 8c. In other

words, the thermal conductivities have less pronounced effects on the convective heat transfer coefficient than on the thermal boundary conditions close to the bottom interface. It may be due to the fact that this interface involves the more complex mass flow and heat transfer by the conjugated porous material and the chemical reactions. It could suggest that more attention is further needed to put on this interface involving the coupled transport processes and chemical reactions if the reformer optimizating design is prevailing.

CONCLUSIONS

A fully three-dimensional CFD code has been further developed to simulate and analyze gas flow and heat transfer processes coupled by the chemical reactions in a composite duct relevant for a compact fuel reformer. The model offers the possibilities of determining temperature and convective heat transfer by taking into account the methane steam reforming, water gas-shift and reverse methanation reactions. It is found that either the averaged temperature gradient (heat flux) or the surface temperature at the top-, side- and bottom interfaces are axially varied along the main flow direction. The small thermal conductivities of the functional materials promote this variation when the other design and operating parameters are kept the same.

ACKNOWLEDGEMENTS

The Swedish Research Council (VR) and the Liaoning Natural Science Foundation of China support the current research.

REFERENCES

[1] R. Farrauto, S. Hwang, L. Shore, W. Ruettinger, J. Lampert, T. Giroux, Y. Liu, O. Ilinich, New Material Needs for Hydrocarbon Fuel Processing: Generating Hydrogen for the PEM Fuel Cell, Annual Review of Material Research 33 (2003) 1-27.

[2] A.L. Dicks, P. Goulding, S.L. Jones, R. Judd, K. Ponton, Assessment of Advanced Catalyst Performance and Fabrication Options for a Compact Steam Reformer, *ETSU F/02/00180/REP, DTI PUB URN 01/1163*, UK, 2001.

[3] M. Zanfir, A. Gavriilidis, Catalytic Combustion Assisted Methane Steam Reforming in a Catalytic Plate Reactor, Chemical Engineering Science 58 (2003) 3947-3960.

[4] D.W. Agar, Multifunctional Reactors: Old Preconceptions and New Dimensions, Chemical Engineering Science 54 (1999) 1299-1305.

[5] V.A. Kirillov, N.A. Kuzin, A.V. Kulikov, S.I. Fadeev, A.B. Shigarov and V.A. Sobyanin, Thermally Coupled Catalytic Reactor for Steam Reforming of Methane and Liquid Hydrocarbons: Experiment and Mathematical Modeling, Theoretical Foundations of Chemical Engineering 37 (2003) 276-284.

[6] J. Yuan, F. Ren and B. Sundén, Analysis of Chemical-Reaction-Coupled Mass and Heat Transport Phenomena in a Methane Reformer Duct for PEMFCs, International Journal of Heat and Mass Transfer, 50 (2007), 687-701.

[7] S.S.E.H. Elnashaie, A.M. Adris, A.S. Al-ubaid and M.A. Soliman, On the Non-monotonic Behaviourof Methane-Steam Reforming Kinetics, Chemical Engineering Sciences, 45 (1990), 491-501.

[8] C.M. Rhie and W.L. Chow, Numerical Study of the Turbulent Flow Past an Airfoil with Trailing Edge Separation, AIAA J. 2 (1983) 1527-1532.

NOMENCLATURE

A_{active} = surface area of control volume at active site, m^2
a = width of porous layer, m
B = inertial coefficient
b = width of flow duct, m
c_p = specific heat, J/(kg K)
D = molar diffusion coefficient of fuel gas species, m^2/s
E_a = activation energy, kJ/mol
H = enthalpy, kJ/mol
h = overall height of the duct, m
h_d = height of the duct, m
h_p = thickness of porous layer, m
J =electrochemical reaction related molar flux, $mol/(m^2 s)$
K_e = equilibrium constants, Pa^2
k =thermal conductivity, W/(m K); reaction rate constant, $mol /(m^3 Pa^2 s)$
k_0 = pre-exponential constant, -
M = molecular weight of species, kg/mol
$\dot{m}$ = mass diffusion flux, $kg/(m^2 s)$
$\dot{n}$ = molar diffusion flux, $mol/(m^2 s)$
Nu = Nusselt number
n = total number of species, -
P = pressure, Pa
q = heat flux, $W/(m^2)$
R = internal reforming reaction rate, $mol/(m^3 s)$
$\Re$ = gas constant, kJ/(mol K)
Re = Reynolds number (UD_h/ν), -
r_e = effective radius, m
S = source term
T = temperature, ^oC
v = velocity vector, m/s
V_i =velocity components in x, y and z directions, respectively, m/s
X = molar fraction of fuel species, -
Y = mass fraction of fuel species, -
x, y, z = Cartesian coordinates

Greek Symbols

β = permeability of porous layer, m^2
ε = porosity, -
μ = dynamic viscosity, kg/(m s)
ν = kinematic viscosity, m^2/s

ρ = density, kg/m^3
τ = tortuosity, -

Superscripts

+ = forward reaction
- = reverse reaction

Subscripts

di = diffusion layer
eff = effective parameter
f = fuel gas mixture
CH_4 = methane
CO = carbon monoxide
CO_2 = carbon dioxide
e = equilibrium
gm = fuel gas mixture
H_2 = hydrogen
H_2O = water
in = inlet
k = Knudsen diffusion
m = mass transfer
p = permeation; porous layer
r = steam reforming reaction
s = solid wall; shift reaction; species